Chemical Engineering Journal 463 (2023) 142117

Contents lists available at ScienceDirect

Chemical Engineering Journal

journal homepage: www.elsevier.com/locate/cej

Contributions of CH_4-amine interactions by primary, secondary, and tertiary amines on CO_2/CH_4 separation efficiency

Basil Wadi [a,b,*], Chenhao Li [c], Vasilije Manovic [a], Peyman Moghadam [c,d], Seyed Ali Nabavi [a,*]

[a] Centre for Renewable and Low Carbon Energy, Cranfield University, Bedford, Bedfordshire MK43 0AL, United Kingdom
[b] Department of Chemical and Biological Engineering, University of Ottawa, Ottawa, Ontario K1N 6N5, Canada
[c] Department of Chemical and Biological Engineering, The University of Sheffield, Sheffield S10 2TN, United Kingdom
[d] Department of Chemical Engineering, University College London, London WC1E 7JE, United Kingdom

ARTICLE INFO

Keywords:
CH_4 separation
Amine grafting
Primary amine
Secondary amine
Tertiary amine
Adsorption

ABSTRACT

In designing amine-incorporated adsorbents for CO_2/CH_4 separation, it is essential to understand the individual effects amine moieties have on the separation of CO_2/CH_4 mixtures. In this work, primary, secondary, and tertiary amines are moderately grafted on SBA-15 to examine factors affecting adsorption of CO_2 and CH_4. Materials were characterised by thermogravimetric and elemental analysis, and their performance was measured by volumetric and gravimetric gas adsorption. An amine density of 1.6–1.7 mmol/g in secondary and tertiary amines showed an equivalent CH_4 uptake of <0.04 mmol/g at 25 °C, while primary amines adsorbed 0.05 mmol/g, indicating stronger interaction forces with CH_4. In terms of selectivity, primary and secondary amines grafted at 1.3–1.4 mmol/g had similar values, unaffected by amine type. Adsorption results cross analysed with DFT simulations indicate similar binding energies for CH_4 by both amine moieties, concluding the facilitated access of gas molecules to primary amine moieties is the primary factor dictating degree of adsorption. At an amine density of ~ 1.7 mmol/g for both primary and secondary amines, an increase in temperature from 25 to 40 °C at a CO_2 partial pressure of 40 kPa showed a decrease in CO_2/CH_4 selectivity of only primary amines. Secondary amines are thus more selective amine moieties at these conditions. Furthermore, in isothermal adsorption–desorption conditions, moderately grafted secondary amines have an equal working capacity to primary amines. Both these qualities support secondary amines at moderate densities as candidates for adsorbent development in CO_2/CH_4 separations.

1. Introduction

Atmospheric CO_2 concentrations continue to rise yearly with the National Oceanic and Atmospheric Administration reporting an annual median of above 410 ppm [1–4]. The increase in atmospheric concentrations of CO_2 from post-industrial anthropogenic emissions has caused reported global warming of ~1.0 °C [5]. There is thus a clear need to decrease greenhouse gas (GHG) emissions to avoid irreversible environmental damage. Sustainable energy sources such as biogas play an essential role in the path towards net-zero carbon emissions. As a result, there has been an increasing interest in utilising cyclic processes that employ Pressure Swing Adsorption (PSA) or Vacuum Swing Adsorption (VSA) for biogas separations. Compared with temperature swing sorption, pressure swing cycle processes benefit from lowered required energy demand, if the utilised adsorbent can offer a maximised CH_4 recovery and minimise regeneration energy [6–8]. Furthermore, the effect of moisture on adsorption efficiency can be resolved upstream or within multibed systems, a practice that is well established and streamlines the treatment and upgrading of biogas streams [9].

In the development of novel adsorbents for carbon capture, the incorporation of amines has been shown to enhance CO_2 capacity and selectivity, shown to be effective at process conditions of up to 10 bar [10–12]. However, many of these applications concentrate on CO_2 adsorption from flue gases in the power and industrial sectors [10,13,14]. With respect to CO_2/CH_4 and biogas mixtures, amines have

Abbreviations: AC, Activated Carbon; APTES, (3-aminopropyl)triethoxysilane; BAPT, (*N*-butylamino)propyl-trimethoxysilane; BdB-FHH, Broekhoff-de Boer - Frenkel-Halsey-Hill; BJH, Barrett-Joyner-Halenda; DFT, Density Functional Theory; DMAPT, dimethylaminopropyl)trimethoxysilane; EA, Elemental analysis; NMR, nuclear magnetic resonance; TGA, Thermogravimetric analysis; UFF, Universal forcefield.

* Corresponding authors at: Centre for Renewable and Low Carbon Energy, Cranfield University, Bedford, Bedfordshire MK43 0AL, United Kingdom (B. Wadi and S.A. Nabavi).

E-mail addresses: bwadi068@uottawa.ca (B. Wadi), s.nabavi@cranfield.ac.uk (S.A. Nabavi).

https://doi.org/10.1016/j.cej.2023.142117
Received 14 November 2022; Received in revised form 9 February 2023; Accepted 21 February 2023
Available online 25 February 2023

Nomenclature

Parameter	Description	Unit
S_{BET}	BET surface area	m^2/g
V_p	Pore volume	cm^3/g
D_p	Pore diameter	nm
$\widehat{S}$	Selectivity	-
ΔH_{Ads}	Isosteric heat of adsorption	J/mol
T	Temperature	K
P	Pressure	kPa
R	Ideal gas constant	J/mol-K
n_s	Toth isotherm parameter	mmol/g
b	Toth isotherm parameter	1/kPa
t	Toth isotherm parameter	-
K	Henry constant	$mol/(m^3 \cdot Pa)$
C_{Des}	Fraction desorbed	-
Ce	Fractional uptake	-
A_x	Adsorption condition at X°C	-
D_x	Desorption condition at X°C	-
q	Molar uptake	mmol/g

the potential to offer exceptional selectivity of CO_2/CH_4, but to the best of our knowledge, only a limited number of studies explore the relationship between amine functionalisation and separation efficiency are available [12,15,16].

Garcia et al. [15] studied the separation of CO_2/CH_4 on amino-grafted silicas, choosing silica as a non-interacting adsorbent base. However, their work was limited to high-density functionalisation, and mainly focused on the adsorption behaviour resulting from different synthesis routes of mesoporous silica. Belmabkhout et al. [17] explored the selectivity of triamine grafted at a high density of 7.9 mmol/gram on MCM-41 through breakthrough experiments. They found that this material achieved an uptake of 1.89 mmol/g. They observed a fast-initial breakthrough of CH_4 in seconds, reporting a selectivity comparable with commercial adsorbents such as Zeolite 5A and BPL activated carbon. Despite this, their study was limited to a CO_2:CH_4 mixture of 1:99 at 100 kPa, and focused on one amine reagent (triamine) targeting maximum CO_2 adsorption enhancement. In a more recent study, Mafra et al. [12] investigated the adsorption of a binary mixture of CO_2/CH_4 across a range of pressures on SBA-15 grafted with a high density of primary, secondary, and diamines to quantify the selectivity of each amine type. They found that secondary amine at a high surface coverage provided the highest selectivity compared to primary amine. However, it was outperformed by primary amines due to its loss in capacity under isothermal desorption conditions of 10 or 100 kPa. They concluded that at the high densities studied, primary amines enhance the capacity and selectivity most effectively, and can be potentially applied for PSA/VSA, but further work is necessary to map out the full range of adsorption mechanisms. Lourenco et al. [18] prepared phenylene-silicas (Ph-PMO) functionalised by various primary amine groups through two methods, by conventional grafting and by strong acid-promoted chemical bonding. They studied the CO_2 and CH_4 interactions by density functional theory (DFT) and found that $-CH_2NH_2$ functionalities on Ph-PMO provide the optimal enhancement of CO_2 uptake without affecting CH_4 adsorption. Although insightful, the work was limited to primary amine groups, while probing the interactions of different amines is yet to be explored.

In terms of functional groups and their effect on CO_2 adsorption, Ko et al. [19] compared the adsorption and desorption behaviour of CO_2 in primary-, secondary-, and tertiary-amine-functionalised SBA-15 at 25 °C, and found that adsorption capacity decreased in the order of Primary > Secondary > Tertiary while desorption followed the opposite trend. In their study, the grafted density was ~3 mmol/g, indicating full surface coverage. Additionally, they used the quantity of CO_2 adsorbed per gram of amine grafted to compare the different amine types, which is representative but does not account for amine spacing and diffusion effects on adsorption efficiency. Moreover, the research was solely based on a pure stream of CO_2, and the effect of adsorption by additional molecules in a binary gas mixture is yet to be explored.

Studies up to this point on the CO_2/CH_4 capture efficiency of amines have shown their potential as adsorbent components that enhance CO_2 capacity and selectivity. However, they have either concentrated on only CO_2-amine mechanisms, primary amines, or on densely grafting different amine types. This work aims to build on this by targeting the individual contribution of each amine moiety or organosilane branch on CH_4 and CO_2 adsorption performance, with a concentration on the contribution of CH_4 interactions on the resulting selectivity. This is accomplished by grafting primary, secondary, and tertiary amines at different densities on SBA-15 and analysing the effects on CO_2/CH_4 selectivity, CH_4 adsorption, isosteric heats of adsorption, and the regeneration energy implications of each amine type. Similar grafting densities have been targeted for an equivalent comparison of the underlying CO_2 adsorption mechanism and the resulting CH_4 interactions by different amine types; narrowing down amine/CH_4-specific influences.

2. Material and methods

2.1. Materials

The different chemical reagents (3-aminopropyl)triethoxysilane (APTES), (N,N-dimethylaminopropyl)trimethoxysilane (DMAPT), toluene (99.8 %), and methanol (HPLC grade) were purchased from Sigma-Aldrich, UK. Additionally, (*N*-butylamino)propyl-trimethoxysilane (BAPT) was purchased from fluorochem. SBA-15 powder was purchased from XFNANO. The methane, nitrogen, and carbon dioxide (99.99 % purity) gases were purchased from BOC, UK.

2.2. Material synthesis

The functionalisation of SBA-15 followed a dry grafting procedure under inert reflux. First, 1 g of SBA-15 powder was dried in a flask under vacuum (40 mbar) at 110 °C for 1 h. The flask and reflux apparatus were then purged with nitrogen, and 80 mL of toluene was added to the flask

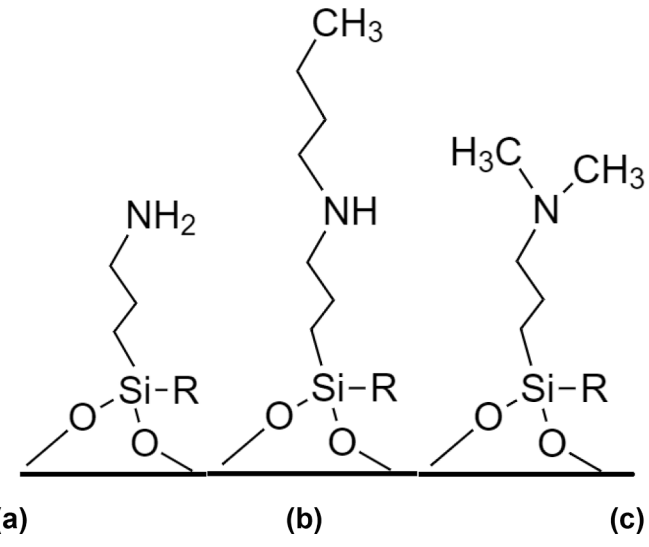

Fig. 1. Silica surface-grafted organo-silanes. R represents the methoxy or ethoxy or hydroxyl group in bidentate grafting. For tridentate grafting, all three Silane branches are bonded to the surface of SBA-15 and R represents surface Si-O-Si bonds. (a) APTES, (b) BAPT, and (c) DMAPT.

followed by the required quantity of amine reagents, illustrated in Fig. 1 and Table 1. The system was heated to 70 °C and left under reflux for 18 h. The grafted SBA-15 powder was recovered by filtering under vacuum suction and washed with ample toluene and methanol. Finally, the samples were left to dry in air at room temperature for 24 h. The samples were labelled as S-x-y with x as type of amine (P-Primary, Sec-Secondary, Te-Tertiary), and y the amine density as measured by elemental analysis (EA), Table 1.

2.3. Material characterisation

Thermogravimetric analysis (TGA 8000, PerkinElmer) and C and N elemental analysis (vario EL III, Elementar) were used to determine the grafted amine density on SBA-15 samples. In the case of TGA, 8–10 mg of each material was exposed to nitrogen at 60 mL/min and heated at a rate of 20 °C/min from 30 °C to 120 °C, held for 10 min, and then increased to 800 °C under the same heating rate. At 800 °C the gas was switched to air and held for an extra 5 min. The weight percent of C and N grafted on SBA-15 was measured by Elemental analysis by thermal combustion analysis using a 10 mg sample.

Structural properties of the samples were estimated from nitrogen adsorption isotherms and are summarised in Table 1. Nitrogen adsorption–desorption isotherms at −196 °C were measured using a 3P *Meso* 222 sorption analyser (3P Instruments). Each sample (0.2–0.3 g) was degassed by heating it under vacuum for 2 h at 90 °C. The Brunauer-Emmett-Teller (BET) method in the relative pressure range of 0.05 to 0.2 was used to calculate the effective surface area [20]. The Barrett-Joyner-Halenda (BJH) method was used to calculate the pore volume of each sample at $p/p^o = 0.95$ [21]. The Broekhoff-de Boer (BdB) method simplified by the Frenkel-Halsey-Hill (FHH) approximation was used for pore size distribution (PSD) estimations [22].

2.4. Adsorption measurements

Gravimetric CO_2 adsorption and desorption measurements at 25 and 40 °C were taken by TGA (TGA 8000, Perkin Elmer) to measure the dynamic uptake of materials. Each sample (8–12 mg) was degassed at 110 °C for 30 min by a 60 mL/min flow of nitrogen and then cooled to 25 °C or 40 °C, depending on the condition required. Upon stabilisation of the temperature, the feed gas was switched to CO_2 at 60 mL/min for 25 min. For the desorption step, the gas was switched to nitrogen at 60 mL/min and the temperature was maintained at 25 or 40 °C for 30 min. For measurements of adsorption at 25 °C and desorption at 40 °C, the temperature was increased to 40 °C at a rate of 15 °C/min and held for 30 min.

CO_2 and CH_4 volumetric adsorption measurements for equilibrium data were carried out using the 3P *Meso* 222 sorption analyser. Each sample (0.25–0.3 g) was degassed under the same procedure previously described for nitrogen adsorption. The sample tube was submerged in a liquid bath (3P Instruments), at a temperature of 25 or 40 °C. A modified form of the two-site Toth isotherm model was applied to fit CO_2 gas adsorption isotherms [23] (Eq. (1)), and the Henry model was used for CH_4 due to the linearity of the adsorption profiles [24,25] (Eq. (2)):

$$q = \left[\frac{n_s b_1 P}{\left(1+(b_1P)^{t_1}\right)^{1/t_1}}\right] + \left[\frac{n_{s2} b_2 P}{\left(1+(b_2P)^{t_2}\right)^{1/t_2}}\right] \quad (1)$$

$$q = KP \quad (2)$$

where n_s, b, and t are the Toth parameters with subscripts to distinguish each adsorption site. The variable K represents the Henry constant. q and P are the molar uptake and pressure.

The isosteric heat of adsorption was calculated using the measured isotherms at 25 or 40 °C and based on the Clausius Clapeyron equation (Eq. (3)) [26]:

$$\ln\frac{P_2}{P_1} = \frac{-\Delta H_{Ads}}{R}\left(\frac{1}{T_2}-\frac{1}{T_1}\right) \quad (3)$$

The isosteric heat of adsorption is represented by H_{Ads}, T_1 and T_2 are the isotherm temperatures of the relative pressures of P_1 and P_2, and R is the universal gas constant.

2.5. Density functional theory (DFT) modelling

For the calculations, we use 1-amino-3-(trihydroxysilyl)propane and 1-butylamine-3-(trihydroxysilyl)propane to represent APTES and BAPT. We performed calculations with the MP2 method and a 6–311 + G(d,p) basis set to compute binding energies of CO_2 and CH_4 with 1-amino-3-trihydroxysilylpropane or 1-butylamine-3-trihydroxysilylpropane. All calculations were performed using the Gaussian 09 package. For each case, to reduce the effects of basis set superposition error we used the counterpoise correction scheme to obtain binding energies. We carried out optimizations for at least two different initial positions of both CO_2 and CH_4 around the 1-amino-3-trihydroxysilylpropane and 1-butylamine-3-trihydroxysilylpropane molecule, and chose the lowest values which also show the correct interaction as the final results. After geometry optimization calculations, the binding energies for CO_2 and CH_4 were calculated according to Eq. (4).

$$\begin{aligned} BE_{molecule} = {} & E_{1-\text{amino}-3-(\text{trihydroxysilyl})\text{propane}(1-\text{butylamine}-3-(\text{trihydroxysilyl})\text{propane})+molecule} \\ & - E_{1-\text{amino}-3-(\text{trihydroxysilyl})\text{propane}(1-\text{butylamine}-3-(\text{trihydroxysilyl})\text{propane})} \\ & - E_{molecule} + E_{BSSE} \end{aligned} \quad (4)$$

where E is the electronic energy, "molecule" is either CO_2 or CH_4 and BSSE is Basis Set Superposition Error correction.

3. Results and discussion

3.1. Physiochemical properties

The BET surface area, pore volume, and maximum encountered pore

Table 1
Physical and chemical properties of raw and functionalised SBA-15.

Sample	Reagent type	Amine type	Reagent added (mmol)	Amine density (mmol/g)		S_{BET} (m^2/g)	Vp (cm^3/g)	Dp (nm)	Silane molecules/nm^2 ‡
				TGA – Tridentate*	EA**				
S-0	–	–		–	–	490	1.2	7.0	–
S-P-1.4	APTES	Primary	2.0	1.49	1.45	406	1.04	6.4	1.79
S-P-1.7	APTES	Primary	4.0	1.78	1.71	308	0.78	6.3	2.10
S-Sec-1.3	BAPT	Secondary	2.0	1.31	1.32	316	0.75	5.8	1.62
S-Sec-1.6	BAPT	Secondary	4.0	1.56	1.56	302	0.69	5.6	1.92
S-Te-1.7	DMAPT	Tertiary	2.0	1.68	1.72	326	0.85	6.3	2.11

‡ Amine coverage calculated from the surface area of S-0 and the total amine density.
* Amine density for tridentate surface bonding from TGA.
**Elemental Analysis.

size of samples are summarised in Table 1. Nitrogen adsorption at −196 °C of raw SBA-15 and functionalised samples resulted in a type IV isotherm associated with mesoporous silicas such as SBA-15 and MCM-41[27,28] (Fig. 2). The PSD maximum confirms the continued mesoporosity of SBA-15 post-functionalisation, with a narrow variation in the range of 5.6 to 7.0 nm the measured values.

Amino organo-silanes can bond with the surface by forming bidentate or tridentate bonds (Fig. 1) [29,30]. From TGA and EA measurements, APTES, BAPT, and DMAPT are more prone to form tridentate bonds under the synthesis conditions used here, as presented in Table 1. The optimal method to ensure the grafting reactions and bonds formed between the amino-organo silianes would be via ss NMR analysis. However, in this work a combination of elemental analysis and TGA were used to predict the most likely type of bonds being formed by the amino-organo silanes. The results indicate mostly tridentate bonds. Although these may be with the surface, studies by Vrancken et al. [29,30] imply the existence of poly condensation too. This is associated with trace water that may be present within the pores and can thus explain the high quantity of 'tridentate' bonds formed by each amino silane, with very few indications of bidentate surface reactions [31]. For all samples, the grafted densities and surface coverage are in-line with previous studies employing similar materials and grafting conditions [12,32–34]. The surface coverage of silane molecules per nm^2 was calculated using the effective surface area of raw SBA-15 and the silane density of each sample.

Although S-P-1.4, S-P-1.7, and S-Te-1.7 have a higher organosilane density compared to S-Sec-1.3, and S-Sec-1.6, a smaller effect on pore volume and specific surface area was observed. The occupation of more pore space by similar densities in the secondary amines is a result of the difference in molecular length between amine types. The overall molecular length was measured using Avogadro (V1.2) based on a Universal Force Field (UFF) geometry optimisation from the base silica to the nitrogen or carbon atom at the end of the molecule. For BAPT, the distance was around 0.89 nm, while it was 0.54 and 0.55 nm for APTES and DMAPT, respectively. Consequently, BAPT occupies more open pore space for similar nitrogen densities. The inherent structure of BAPT limited the achievable grafted density to a maximum of 1.56 mmol/g, compared to 2.6 mmol/g for APTES, as previously reported [31].

3.2. Adsorption performance

The adsorption isotherms measured for CO_2 and CH_4 at 25 and 40 °C are presented in Fig. 3. The change in the CH_4 adsorption profile of the different functionalities provides a comparative analysis of the effects of porosity and amine type on adsorbent performance in CO_2:CH_4 mixtures (Fig. 3b and d). A clear decrease in CH_4 uptake is seen as amine surface density increases. However, the extent of the reduction depended on amine type. To scrutinise the reason for these differences, the CH_4 capacity at 25 °C and 100 kPa of all the materials is correlated with the pore volume and silane surface coverage and is presented in Fig. 4.

Referring to Fig. 4a and b, the adsorption capacity of primary amines at similar surface coverage deviated from the rest of the samples. In primary amine samples, the increase in silane functionalisation from raw SBA-15 did not decrease CH_4 adsorption to the same degree as secondary and tertiary amines. Although, at a higher temperature of 40 °C (Fig. 4b), the differences between the primary and secondary amines are less pronounced, due to the lower overall uptake from weak interactions between the amines and CH_4. The differences in the adsorption of CH_4 by APTES could be attributed to the shorter overall molecular length which would create more pore space under similar densities.

To further scrutinise the parameters affecting CH_4 adsorption, the CH_4 uptake at 100 kPa correlated with each sample's pore volume at 25 and 40 °C is presented in Fig. 4c and d. From the scattered distribution of CH_4 uptake in Fig. 4c, there is no definite effect caused by only pore volume at these conditions (100 kPa and 25 °C). The pore volume at similar densities is in the order of S-Te-1.7 > S-P-1.7 > S-Sec-1.6, but the quantity of adsorbed CH_4 is highest for S-P-1.7 and lowest for S-Sec-1.6.

Similarly, within the same amine types, there is a greater decrease in CH_4 uptake when amine density increases in secondary amines compared to primary amines. From S-Sec-1.3 to S-Sec-1.6, the pore volume decreased by 0.06 cm^3/g, while from S-P-1.4 to S-P-1.7 it decreased by 0.26 cm^3/g. The small volume change in BAPT resulted in a decrease in CH_4 uptake by 37 % in S-Sec-1.3 and by 47 % in S-Sec-1.6. For APTES, despite a larger variation in pore volume observed from S-P-1.4 to S-P-1.7, the difference in CH_4 uptake was negligible. At this temperature, the small change in CH_4 uptakes may indicate that methane has a higher interaction with APTES moieties, compared to BAPT and DMAPT.

For adsorption at 40 °C, an imposed linear average can be drawn amongst all samples, indicating that a relationship exists between the adsorbed CH_4 and the pore volume (Fig. 4d). Higher adsorption temperatures affect physiosorbed molecules following Le Chatelier's principle, by shifting the equilibrium away from the adsorbent surface and towards the gas phase. This is partially due to an increase in the internal energy of adsorbate molecules at higher temperature that weakens electrostatic interaction with the adsorbent. CH_4 does not contain a quadrupole moment, but there is a surface interaction between adsorbate and adsorbent due its octupole moment. This makes CH_4 a weakly adsorbing molecule, but the changes in the adsorption profile with temperature amongst different amine reagents can allow scrutiny of the intermolecular interactions between amine and CH_4. For APTES, the increase in temperature resulted in a decrease in the uptake of S-P-1.7 from S-0 by 47 %. This reduction is considerably higher compared to S-Sec-1.3 and S-Sec-1.6, decreasing 15 % and 33 %, respectively.

There is a lower effect on CH_4 uptake at 40 °C between the functionalised and raw SBA-15 compared to 25 °C. The higher dependency on temperature of CH_4 uptake by APTES is facilitated by the accessibility of CH_4 to surface amine moieties in APTES due to its location at the tip of the organosilane branch instead of in the middle as is the case with BAPT. It's important to note that at the lowest APTES density (S-P-1.4)

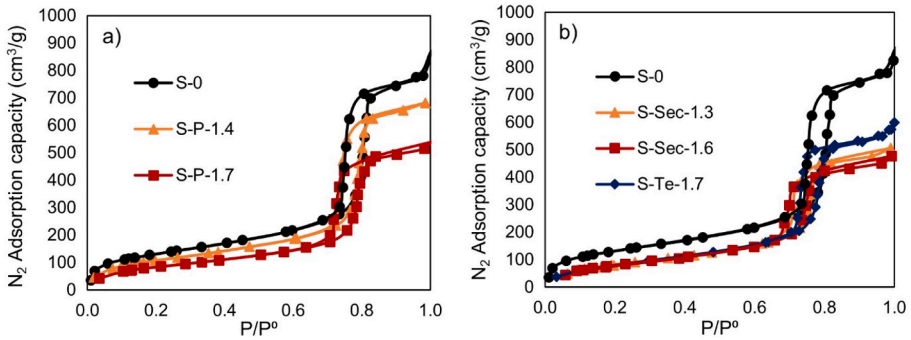

Fig. 2. Nitrogen adsorption–desorption isotherm at −196 °C for raw and (a) APTES, and (b) BAPT and DMAPT functionalised SBA-15.

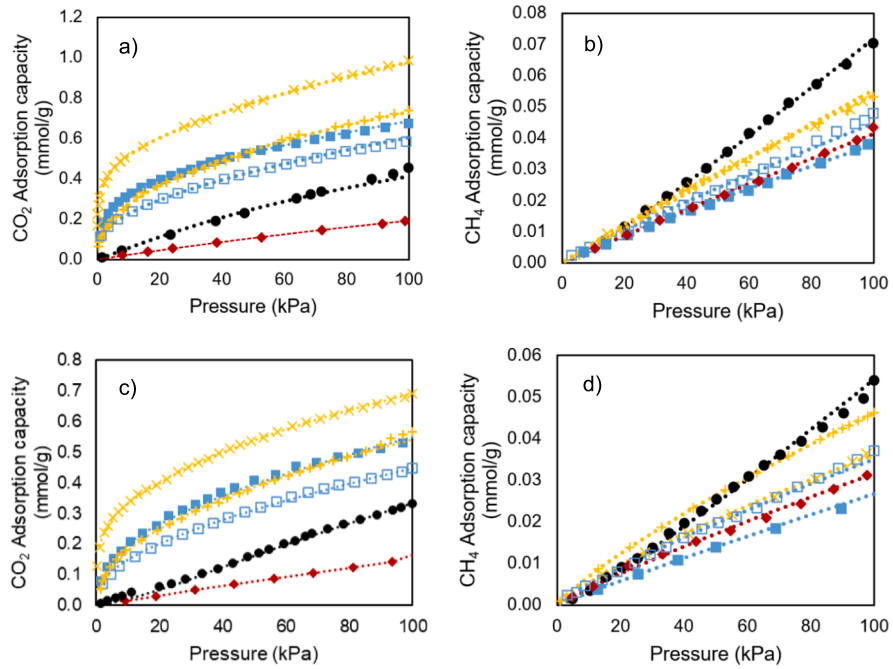

Fig. 3. Adsorption isotherms of functionalised materials for (a) CO_2 and (b) CH_4 at 25 °C, and (c) CO_2 and (d) CH_4 at 40 °C. *The lines represent the model fit and the following markers represent the experimental data:* (●) S-0, (+) S-P-1.4, (X) S-P-1.7, (□) S-Sec-1.3, (■) S-Sec-1.6, (◆) S-Te-1.7.

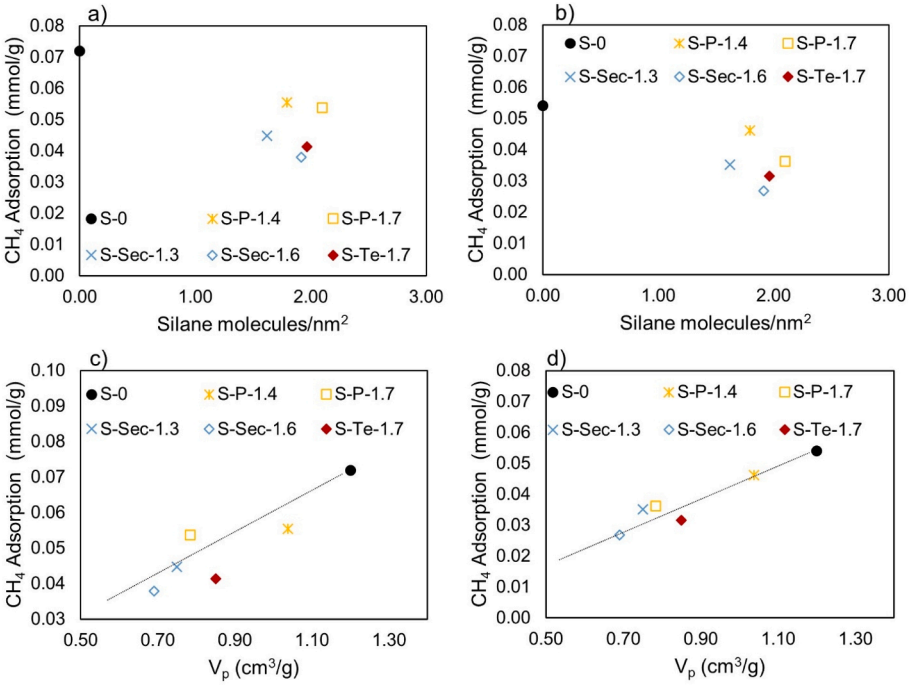

Fig. 4. Relationship between CH_4 equilibrium capacity at 100 kPa with (a) silane surface coverage at 25 °C and (b) silane surface coverage at 40 °C, and with (c) pore volume at 25 °C and (d) pore volume at 40 °C. (●) S-0, (✳) S-P-1.4, (□) S-P-1.7, (X) S-Sec-1.3, (◇) S-Sec-1.6, (◆) S-Te-1.7.

the change of temperature resulted in the same uptake as S-Sec-1.3, a maximum of 0.5 mmol/g at 100 kPa. This is likely a result of the large pore volume of S-P-1.4, and any possible changes to electrostatic forces affecting CH_4 adsorption are less distinguishable.

To further understand the degree off effect by molecular interactions versus amine accessibility, DFT calculations were performed. The interactions of methane are primarily a result of induced dipole effects or London dispersion forces, but due to the non-polar nature of methane, uncertainties can arise as to the exact extent of the molecular interactions [35]. The binding or interaction energy ($\Delta E_{binding}$) and optimised structures studied are presented in Fig. 5. The CH_4 molecule tends closer to the amine moieties in both organosilanes. Although with only small differences, CH_4 imposed on –NH- moieties show a higher interaction energy, a 3.5 kJ/mol difference compared with $–NH_2$, which may indicate a higher affinity of CH_4 to secondary amines, a characteristic that should be kept in mind and further studied. However, considering the molecular length of BAPT at equivalent densities of APTES, a larger percentage of CH_4 is restricted from approaching the secondary amine group. As a result, it interacts instead with only the methyl groups at the end of the BAPT molecule. This may explain the differences in CH_4 uptake seen. Nonetheless, it is important to account for surface bonding - an important phenomenon shown to have a contributing effect on adsorption through bonding between functional groups and surface hydroxyls, as shown by work within the literature [36,37]. In this work, the simulation ignored the surface of the adsorbent, which may have a contributing effect but the work seeks to isolate the contribution of amines for applications beyond silica-based adsorbents.

These findings are in agreement with a recent study by Lourenco et al. [18], performing DFT analysis on the interaction energy of CH_4 with primary amines grafted on Ph-PMO. They found noticeable differences in the degree of interactions of CH_4 based on the type of amine. The in-detail study of surface influences, hydrogen bonding, and degree of CH_4 interaction based on low to high alkylamine loadings is necessary. However, this can be computationally expensive and is the basis of a separate publication in and of itself.

With respect to the CO_2 adsorption behaviour of the synthesised materials, similar quantities of grafted total amines among APTES, BAPT, and DMAPT allows for a like-for-like comparison of the adsorption behaviour of each amine type (Fig. 3a and c). Ko et al. [19] previously compared the performance of these amines using amine efficiency, defined as CO_2 adsorbed per N mmol grafted. However, closely examining CO_2 adsorption between amines under equal amine loading can clarify contributions not just from chemisorption but also the physisorption of CO_2. Comparing S-Sec-1.6 and S-P-1.7, the primary amine outperforms secondary amine-grafted samples, showing higher amine efficiency in primary amines at this density; in agreement with results by Ko et al. [19]. This further confirms the importance of amine accessibility in CO_2 adsorption, since although higher individual interaction energies were calculated for secondary amines using DFT, primary amines showed better efficiency in experimental results (Fig. 5). The tertiary amine, S-Te-1.7, adsorbed a lower quantity of CO_2 than raw SBA-15 and, therefore, a limited number of measurements were carried out for it. It has been shown that tertiary amines could adsorb CO_2 and form bicarbonate in "dry" conditions but at negligible quantities of <0.01 mmol/g [38]. This results in a low capture capacity due to the reduced surface area and hinders any physisorption seen in raw SBA-15. The studies presented here target an understanding of amines for pre-dried biogas feeds, and so the influence of moisture on the efficiency of each amine is out of the scope of this work.

The samples with lower amine density, S-P-1.4 and S-Sec-1.3, present almost identical adsorption capacity (~0.13 mmol/g) below 13 kPa (at 25 °C) before S-Sec-1.3 diverges into a gentler slope. This behaviour is similarly seen at 40 °C but the divergence commences at a lower pressure (Fig. 3c). The widening gap in CO_2 uptake between the two samples is likely a result of diffusion hindrance caused by the bulkier BAPT molecules and lower silane surface coverage. The lower quantity of adjacent amines in S-Sec-1.3 provides fewer active sites for the pairwise chemisorption of CO_2 and a faster transition to physisorption. During this transition to physisorption, the lower pore volume hinders

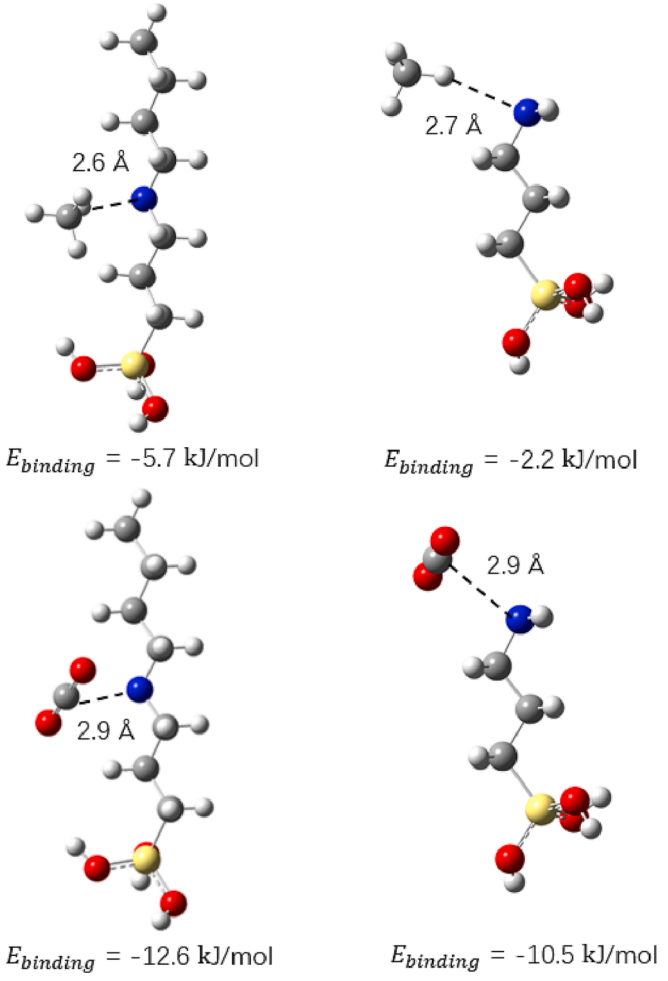

Fig. 5. The lowest energy configurations of methane (top) and carbon dioxide (bottom) interacting with an isolated 'BAPT' (left) or 'APTES' (right) representative molecule. The results are predicted at the MP2/6–311+(d,p) level of theory. The number in the middle of each structure shows the distance between two atoms in Å and the number below shows the binding energy in kJ/mol.

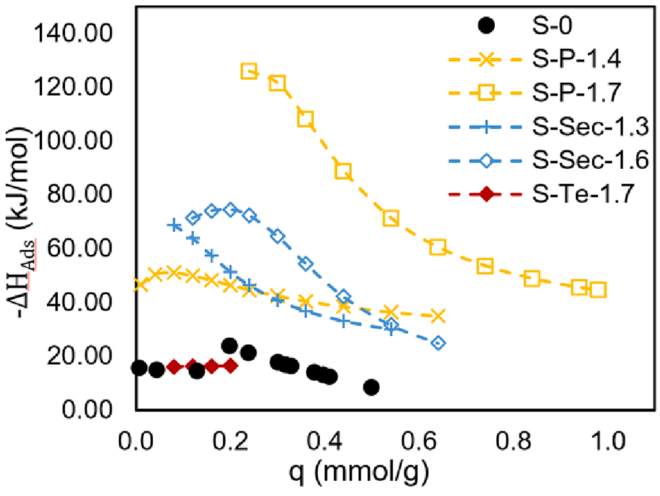

Fig. 6. CO_2 isosteric heat of adsorption of the functionalised materials.

CO_2 diffusion and rationalises the increasing difference in uptake between S-Sec-1.3 and S-P-1.4 as pressure increases. This is supported by the calculated heat of adsorption in Fig. 6, in which S-Sec-1.3 crosses S-P-1.4 at a CO_2 loading above 0.2 mmol/g, indicating a larger contribution from physisorption within this region.

From these results, it can be concluded that primary and secondary amines at low coverage can lead to the same adsorption capacity at low CO_2 pressures. The lower quantity of adjacent amines in S-Sec-1.3 provides fewer active sites for the pair-wise chemisorption of CO_2. Additionally, it has been proposed by Hahn et al. [39] that energetically less favoured carbamic acid is more likely to form at low loadings of primary and secondary amines as adjacent amine pairs decrease in number. This means that they undergo similar adsorption mechanisms regardless of the amine type. This implies that the efficiency of amines in capturing CO_2 may not always agree with higher brute force capacity, adsorbent loadings, and pressures.

3.3. Adsorption selectivity

To understand the effect of amine functionalisation on the selective adsorption of CO_2, the developing CO_2/CH_4 static selectivity ($\widehat{S}$) with CO_2 partial pressure was calculated using Eq. (5) at 25 °C, up to 100 kPa, and is presented in Fig. 7.

$$\widehat{S} = \frac{q_i/P_i}{q_j/P_j} \tag{5}$$

All the functionalised secondary and primary amine samples have a similar rate of decrease in selectivity as partial pressure of CO_2 increases. At a CO_2 partial pressure of 40 kPa, the selectivity of S-P-1.4, S-P-1.7, S-Sec-1.3, and S-Sec-1.6 is 22, 33, 23, and 32, respectively, a significant increase from S-0 of 7.5. We compare the selectivity at lower CO_2 partial pressures, as it represents the dynamic adsorption along an adsorbent bed in which lower partial pressures are expected near the bed outlet. In this case, S-P-1.7 achieves a higher selectivity than secondary amines at similar densities, 252(for S-P-1.7) versus 192 (for S-Sec-1.6) at a $P_{CO2} =$ 3 kPa. Contrary to that, S-Sec-1.3 shows better selectivity than its primary counterpart, with 108 versus 95 (S-P-1.4) at $P_{CO2} = 3$ kPa.

In the previous section, it was concluded that there is a negligible difference in selectivity based on amine type. However, referring to Fig. 8, there seems to be a correlation between amine density and selectivity, but irrelevant of amine type. The selectivity at 25 °C increases in the order of S-Sec-1.3 <S-P-1.4 <S-Sec-1.6 <S-P-1.7, showing dependence on only the amine density. The primary contributions to the change in selectivity are illustrated in Fig. 9, which compares the calculated selectivity with the pure gas adsorption of CO_2 and CH_4 at pressures of 40 and 60 kPa, respectively. When APTES and BAPT are grafted at similar densities, the ratio of CO_2 to CH_4 adsorbed is mirrored, causing the similarity in selectivity observed.

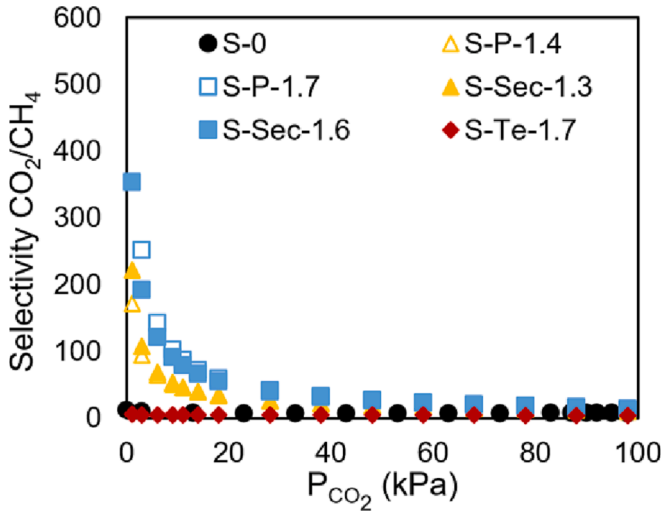

Fig. 7. Selectivity at 25 °C of APTES, BAPT and DMAPT.

At 40 °C, the order of increase in selectivity is altered towards S-P-1.4 (18) <S-Sec-1.3 (19) <S-P-1.7 (29) <S-Sec-1.6 (33), and is presented in Fig. 8b. Although by a small fraction, the selectivity of primary amines decreased on a higher magnitude compared to secondary amines. The previous section demonstrated that temperature had a greater effect on the CH_4 adsorption of APTES-functionalised materials. Additionally, at higher temperatures primary amines showed the largest decrease in CO_2 adsorption at a partial pressure of 40 kPa. The combined effect of a lower CO_2 and CH_4 uptake at higher temperatures explains the greater effect on selectivity seen in APTES-functionalised samples.

3.4. Regeneration efficiency

Grafted samples with a maximum density of primary amines provide the highest CO_2 adsorption capacity and selectivity. On the other hand, it significantly increases the heat of adsorption, and in turn energy demand for regenerations. This is reflected in the adsorption–desorption cycles under isothermal and non-isothermal conditions presented in Fig. 10 and Table 2. S-P-1.7 has a higher CO_2 uptake (0.53 mmol/g) compared to S-Sec-1.6 (0.4 mmol/g) but an equivalent quantity in both adsorbents of 0.36 mmol/g of CO_2 under is desorbed following a nitrogen purge at 1 bar. Additionally, the desorption kinetics of S-Sec-1.6 are the fastest and lead to the highest fraction of adsorbent 'regeneration' (C_{Des}) under isothermal conditions at 25 °C (Fig. 10). At non-isothermal conditions of 25 °C adsorption to 40 °C desorption (Table 2), S-P-1.7 outperforms the secondary amine and desorbs 0.48 mmol/g compared to 0.39 mmol/g for S-Sec-1.6. This is a result of the formation of carbamates with a strong intramolecular stabilisation in primary amines. The existence of these species has been shown to be a characteristic of chemisorption by higher density primary amines [40]. The stronger stabilisation of chemisorbed species leads to higher heats of adsorption and a greater dependency on temperature for desorption. This is in agreement with previous studies showing that the secondary amine [3-(methylamino) propyl] trimethoxysilane required lower energy for regeneration compared to (3-aminopropyl) trimethoxysilane under similar conditions [19]. The combination of energy efficiency and the enhanced selectivity towards CO_2 of secondary amines can make them a competitive option for biogas separations in a VPSA/PSA arrangement. In all cases, the cyclability of grafted amines has already been demonstrated within literature and has therefore been omitted from this work [10,14,17].

In addition, there is a slight discrepancy in adsorption capacity between TGA measurements and equilibrium isotherm measurements. This is likely explained by the two different adsorption mechanisms at play. At CO_2 partial pressures below 20 kPa, chemisorption dominates and a fast adsorption kinetics results. As the partial pressure increases, physisorption dominates and a slow approach towards equilibrium follows. The difference is up to 0.3 mmol/g and highlights the significant contribution a physisorption to the capacity of these absorbance, as well as the limitation in adsorption kinetics at higher partial pressures.

The low calculated heats of adsorption, faster desorption kinetics, and ease of desorption make secondary amines an interesting component to consider for future adsorbent development.

Current benchmark adsorbents within literature generally achieve higher adsorption capacities compared to amine grafted silicas. Examples include Zeolite ZSM-5 with 1.78 mmol/g CO_2 capacity or Pine SawDust Activated Carbon (AC) at 2.00 mmol/g [41,42]. Nonetheless, the selectivity of amine grafted materials is what places them in a position of interest. Even at the highest degree of CH_4 adsorption, the capacity does not exceed 0.045 mmol/g within this study, in stark comparison with CH_4 capacities of 0.35 to 0.83 mmol/g at 100 kPa by benchmark materials (Table S1 in Supporting Information). In terms of

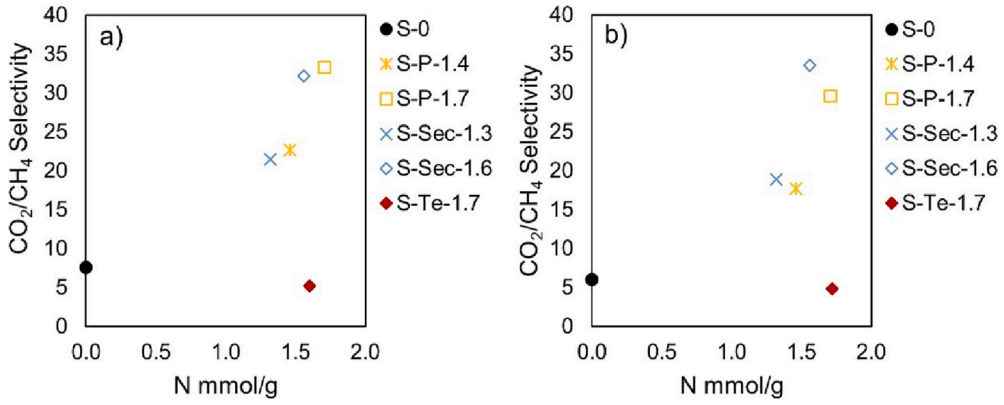

Fig. 8. Effect of amine density on CO_2/CH_4 selectivity at a CO_2 partial pressure of 40 kPa (a) 25 °C, and (b) 40 °C.

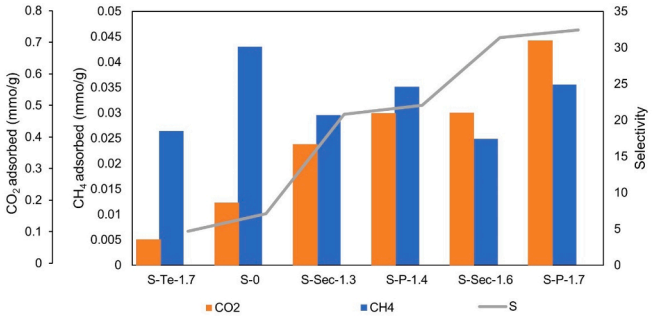

Fig. 9. The CO_2 and CH_4 adsorption capacity at 40 kPa and 60 kPa from pure gas adsorption isotherms compared to the calculated selectivity at P_{CO2} of 40 kPa and 25 °C. '*S*' represents selectivity.

cost, amine functionalised silicas are considered an expensive material compared to AC and zeolites. Preliminary costing estimates a manufacturing cost of £900-4000 per ton of Amino-silicas compared to below £550 per ton of ZSM-5 [43]. However, the goal of this paper is to present a deeper understanding of the developing effect on selectivity by amine functionalities. Through this, new materials can be tailored with controlled quantities of amines, such as nitrogen doped polymeric beads. In this manner, selectivity may be optimized for biogas separations, allowing for the development of novel gas separation processes.

The low regeneration duty is accompanied by an enhanced capacity and selectivity that at the right surface coverage could be applied to biogas separation applications. Nonetheless, further studies exploring the adsorption profiles of low to moderately functionalised adsorbent at higher pressures should be undertaken. The moderate densities could make isothermal regenerations more effective in employing amine functionalisation. Moderate functionalisation provides a balanced level of enhancement in capacity and selectivity while minimising capacity loss in cyclic operations.

4. Conclusions

This study scrutinized the role of CH_4 interactions in adsorbent selectivity of various amine moieties and densities grafted on a surface. The selectivity was then correlated to CO_2 adsorption capacities and the adsorbent's surface morphology to identify key variables influencing selectivity. The optimal amine modification was then identified through an analysis of the efficacity of amine regeneration. A comparison of the adsorption capacity of CO_2 on primary and secondary amines at similar densities showed that an amine's adsorption efficiency is affected only by CO_2 partial pressure. Regardless of the amine, low amine densities give rise to similar CO_2 adsorption capacities at pressures below 10 kPa. For CH_4 adsorption, secondary and tertiary amines at similar surface coverage showed small differences in CH_4 uptake, indicating that for

Table 2
Isothermal and non-isothermal adsorption–desorption runs of selected samples.

	S-Sec-1.6		S-P-1.4		S-P-1.7	
	A_{25}-D_{25}	A_{25}-D_{40}	A_{25}-D_{25}	A_{25}-D_{40}	A_{25}-D_{25}	A_{25}-D_{40}
q_{Ads} (mmol/g)	0.40	0.39	0.33	0.30	0.53	0.50
q_{Des} (mmol/g)	0.36	0.39	0.26	0.30	0.36	0.48
C_{Des}	0.90	1.00	0.80	1.00	0.69	0.96

q_{Ads} – CO_2 adsorbed at 30 min of CO_2 flow.
q_{Des} – CO_2 desorbed after 30 min of N_2 flow.
C_{Des} – Fraction of adsorbed CO_2 that is desorbed (**q_{Des} / q_{Ads}**).
A_{25} and **A_{40}:** Adsorption at 25 °C and 40 °C, respectively.
D_{25} and **D_{40}:** Desorption at 25 °C and 40 °C, respectively.

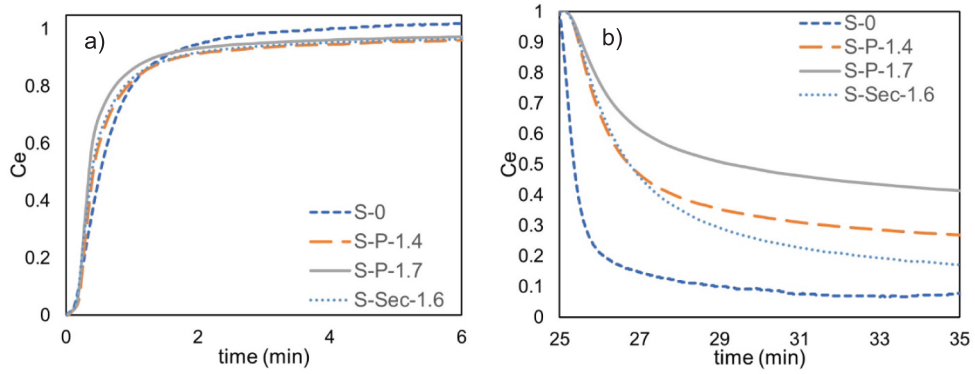

Fig. 10. CO_2 (a) adsorption and (b) desorption curves at 25 °C and 100 kPa. *Ce* represents the fractional uptake of CO_2 out of a total adsorption of q_{Ads}.

these materials, the accessibility of amine branches within the adsorbent's pore is the main influence on CH_4 adsorption. When comparing primary amines to secondary and tertiary amines, a smaller decrease in CH_4 adsorption is seenas amine density increases. These results confirm the presence of higher amine-adsorbate interactions in primary amines. The DFT analysis indicates that its likely due to the unhindered approach of CH_4 molecules to primary amine moieties, since slightly higher interaction energies were calculated for secondary amine moieties. Further computational studies on surface bonding and amine density must be carried out to elucidate the direct individual molecular level influences, but is beyond the scope of this paper and is the basis of its own work. Overall, for primary and secondary amines, the effect of amine type on the selectivity of CO_2 at partial pressures of 40 kPa up to 100 kPa was negligible, displaying instead a correlation with amine density. Although primary amines have been shown to have the highest CO_2/CH_4 selectivity and capacity, the associated desorption and energy demands for regenerations reduces their efficiency for vacuum swing adsorption applications. This is a result of incomplete regeneration, making the excess amines incorporated purposeless. For moderately grafted amines under isothermal applications, secondary amines are viable alternatives that provide comparable capacity and superior selectivity, while simultaneously maintaining a lower energy penalty for CO_2/CH_4 separations. The low influence of temperature on desorption is key in designing carbon capture processes that aim to minimise overall process energy demands.

Declaration of Competing Interest

The authors declare that they have no known competing financial interests or personal relationships that could have appeared to influence the work reported in this paper.

Data availability

No data was used for the research described in the article.

Acknowledgement

The authors would like to thank Howard Smith, Euan Hakon, Jane Hubble, Maria Biskupska, and Richard Andrews for their help and support during the entire experimental campaign.

Appendix A. Supplementary data

Supplementary data to this article can be found online at https://doi.org/10.1016/j.cej.2023.142117.

References

[1] R.B. Jackson, P. Friedlingstein, R.M. Andrew, J.G. Canadell, C. Le Quéré, G. P. Peters, Persistent fossil fuel growth threatens the Paris Agreement and planetary health, Environ. Res. Lett. 14 (12) (2019) 121001.
[2] G.P. Peters, R.M. Andrew, J.G. Canadell, P. Friedlingstein, R.B. Jackson, J. I. Korsbakken, C. Le Quéré, A. Peregon, Carbon dioxide emissions continue to grow amidst slowly emerging climate policies, Nat. Clim. Chang. 10 (2020) 3–6, https://doi.org/10.1038/s41558-019-0659-6.
[3] P. Friedlingstein, M. O'Sullivan, M.W. Jones, R.M. Andrew, J. Hauck, A. Olsen, G.P. Peters, W. Peters, J. Pongratz, S. Sitch, Global carbon budget 2020, Earth Syst. Sci. Data. 12 (2020) 3269–3340.
[4] N. Dr. Pieter Tans, scripps institution of oceanography Dr. Ralp Keeling, NOAA/GML, (2021). www.esrl.noaa.gov/gmd/ccgg/trends/ (accessed January 15, 2021).
[5] T.W. (eds. . Masson-Delmotte, V., P. Zhai, H.-O. Pörtner, D. Roberts, J. Skea, P.R. Shukla, A. Pirani, W. Moufouma-Okia, C. Péan, R. Pidcock, S. Connors, J.B.R. Matthews, Y. Chen, X. Zhou, M.I. Gomis, E. Lonnoy, T. Maycock, M. Tignor, IPCC, 2018: Global Warming of 1.5°C., Intergovernmental Panel on Climate Change (IPCC), 2019. https://www.ipcc.ch/site/assets/uploads/sites/2/2019/06/SR15_Full_Report_Low_Res.pdf.
[6] N. Scarlat, J.-F. Dallemand, F. Fahl, Biogas: developments and perspectives in Europe, Renew. Energy. 129 (2018) 457–472, https://doi.org/10.1016/j.renene.2018.03.006.
[7] A.S. Bhown, B.C. Freeman, Analysis and status of post-combustion carbon dioxide capture technologies, Environ. Sci. Technol. 45 (2011) 8624–8632, https://doi.org/10.1021/es104291d.
[8] L. Joos, J.A. Swisher, B. Smit, Molecular simulation study of the competitive adsorption of H2O and CO_2in zeolite 13X, Langmuir 29 (2013) 15936–15942, https://doi.org/10.1021/la403824g.
[9] A. Golmakani, S. Ali Nabavi, B. Wadi, V. Manovic, Advances, challenges, and perspectives of biogas cleaning, upgrading, and utilisation, Fuel. 317 (2022), 123085, https://doi.org/10.1016/j.fuel.2021.123085.
[10] X.(. Hu, L. Liu, X. Luo, G. Xiao, E. Shiko, R. Zhang, X. Fan, Y. Zhou, Y. Liu, Z. Zeng, C. Li, A review of N-functionalized solid adsorbents for post-combustion CO_2 capture, Appl. Energy. 260 (2020) 114244.
[11] Y. Meng, J. Jiang, Y. Gao, A. Aihemaiti, T. Ju, Y. Xu, N. Liu, Biogas upgrading to methane: Application of a regenerable polyethyleneimine-impregnated polymeric resin (NKA-9) via CO_2sorption, Chem. Eng. J. 361 (2019) 294–303, https://doi.org/10.1016/j.cej.2018.12.091.
[12] L. Mafra, T. Čendak, S. Schneider, P.V. Wiper, J. Pires, J.R.B. Gomes, M.L. Pinto, Amine functionalized porous silica for CO_2/CH4 separation by adsorption: Which amine and why, Chem. Eng. J. (2018) 612–621, https://doi.org/10.1016/j.cej.2017.12.061.
[13] A. Samanta, A. Zhao, G.K.H. Shimizu, P. Sarkar, R. Gupta, Post-combustion CO 2 capture using solid sorbents: A review, Ind. Eng. Chem. Res. 51 (2012) 1438–1463, https://doi.org/10.1021/ie200686q.
[14] E.E. Ünveren, B.Ö. Monkul, Ş. Sarıoğlan, N. Karademir, E. Alper, Solid amine sorbents for CO_2 capture by chemical adsorption: A review, Petroleum 3 (2017) 37–50, https://doi.org/10.1016/j.petlm.2016.11.001.
[15] E. Vilarrasa-García, J.A. Cecilia, M. Bastos-Neto, C.L. Cavalcante, D.C.S. Azevedo, E. Rodriguez-Castellón, CO_2/CH_4adsorption separation process using pore expanded mesoporous silicas functionalizated by APTES grafting, Adsorption 21 (8) (2015) 565–575.
[16] L. Pino, C. Italiano, A. Vita, C. Fabiano, V. Recupero, Sorbents with high efficiency for CO_2 capture based on amines-supported carbon for biogas upgrading, J. Environ. Sci. (China) 48 (2016) 138–150, https://doi.org/10.1016/j.jes.2016.01.029.
[17] Y. Belmabkhout, R. Serna-Guerrero, A. Sayari, Adsorption of CO_2-containing gas mixtures over amine-bearing pore-Expanded MCM-41 silica: application for gas purification, Ind. Eng. Chem. Res. 49 (2010) 359–365, https://doi.org/10.1021/ie900837t.
[18] M.A.O. Lourenço, C. Siquet, M. Sardo, L. Mafra, J. Pires, M. Jorge, M.L. Pinto, P. Ferreira, J.R.B. Gomes, Interaction of $CO_2$and CH4 with functionalized periodic mesoporous phenylene–silica: periodic DFT calculations and gas adsorption measurements, J. Phys. Chem. C. 120 (2016) 3863–3875, https://doi.org/10.1021/acs.jpcc.5b11844.
[19] Y.G. Ko, S.S. Shin, U.S. Choi, Primary, secondary, and tertiary amines for CO_2 capture: Designing for mesoporous CO_2 adsorbents, J. Colloid Interface Sci. 361 (2011) 594–602, https://doi.org/10.1016/j.jcis.2011.03.045.
[20] F. Rouquerol, J. Rouquerol, K. Sing, Adsorption by powders and porous solids, Academic Press, London, 1999.
[21] A.V. Neimark, P.I. Ravikovitch, M. Grün, F. Schüth, K.K. Unger, Pore size analysis of MCM-41 type adsorbents by means of nitrogen and argon adsorption, J. Colloid Interface Sci. 207 (1998) 159–169, https://doi.org/10.1006/jcis.1998.5748.
[22] W.W. Lukens, P. Schmidt-Winkel, D. Zhao, J. Feng, G.D. Stucky, Evaluating pore sizes in mesoporous materials: a simplified standard adsorption method and a simplified Broekhoff–de Boer method, Langmuir. 15 (1999) 5403–5409, https://doi.org/10.1021/la990209u.
[23] R. Serna-Guerrero, Y. Belmabkhout, A. Sayari, Modeling CO_2 adsorption on amine-functionalized mesoporous silica: 1. A semi-empirical equilibrium model, Chem. Eng. J. 161 (2010) 173–181, https://doi.org/10.1016/j.cej.2010.04.024.
[24] O. Talu, A.L. Myers, Rigorous thermodynamic treatment of gas adsorption, AIChE J. 34 (11) (1988) 1887–1893.
[25] D.M. Ruthven, Principles of adsorption and adsorption processes, John Wiley & Sons, 1984.
[26] D.M. Young, A.D. Crowell, Physical Adsorption of gases, Butterworths, London, 1962.
[27] D.D. Do, Adsorption analysis: equilibria and kinetics, Imperial college press London, 1998.
[28] M. Thommes, K. Kaneko, A.V. Neimark, J.P. Olivier, F. Rodriguez-Reinoso, J. Rouquerol, K.S.W. Sing, Physisorption of gases, with special reference to the evaluation of surface area and pore size distribution (IUPAC Technical Report), Pure Appl. Chem. 87 (2015) 1051–1069, https://doi.org/10.1515/pac-2014-1117.
[29] K.C. Vrancken, P. Van der Voort, I. Gillis-d'Hamers, E.F. Vansant, Influence of Water in the reaction of y-Aminopropyltriethoxysilane with Silica Gel, J. Chem. Soc. Faraday Trans. 88 (1992) 3197–3200. doi: 10.1039/FT9928803197.
[30] K.C. Vrancken, P. Van Der Voort, K. Possemiers, E.F. Vansant, Surface and structural properties of silica gel in the modification with $γ $-aminopropyltriethoxysilane, J. Colloid Interface Sci. 174 (1995) 86–91, https://doi.org/10.1006/jcis.1995.1367.
[31] B. Wadi, A. Golmakani, V. Manovic, A. Nabavi, Effect of combined primary and secondary amine densities on the adsorption mechanism of CO2 and CH4, Chem. Eng. J. 420 (2021), https://doi.org/10.1016/j.cej.2021.130294.
[32] K. Hori, T. Higuchi, Y. Aoki, M. Miyamoto, Y. Oumi, K. Yogo, S. Uemiya, Effect of pore size, aminosilane density and aminosilane molecular length on CO_2adsorption performance in aminosilane modified mesoporous silica, Microporous Mesoporous Mater. 246 (2017) 158–165, https://doi.org/10.1016/j.micromeso.2017.03.020.

[33] T. Watabe, K. Yogo, Isotherms and isosteric heats of adsorption for CO_2in amine-functionalized mesoporous silicas, Sep. Purif. Technol. 120 (2013) 20–23, https://doi.org/10.1016/j.seppur.2013.09.011.
[34] C.J. Yoo, S.J. Park, C.W. Jones, CO_2 Adsorption and Oxidative Degradation of Silica-Supported Branched and Linear Aminosilanes, Ind. Eng. Chem. Res. 59 (2020) 7061–7071, https://doi.org/10.1021/acs.iecr.9b04205.
[35] D.R. Johnston, G.J. Oudemans, R.H. Cole, Dielectric Constants of Imperfect Gases. I. Helium, Argon, Nitrogen, and Methane, J. Chem. Phys. 33 (1960) 1310–1317. doi: 10.1063/1.1731405.
[36] L. Mafra, T. Ċendak, S. Schneider, P.V. Wiper, J. Pires, J.R.B. Gomes, M.L. Pinto, Structure of chemisorbed CO_2 species in amine-functionalized mesoporous silicas studied by solid-state NMR and computer modeling, J. Am. Chem. Soc. 139 (1) (2017) 389–408, https://doi.org/10.1021/jacs.6b11081.
[37] E. De Canck, I. Ascoop, A. Sayari, P. Van Der Voort, Periodic mesoporous organosilicas functionalized with a wide variety of amines for CO2 adsorption, Phys. Chem. Chem. Phys. 15 (2013) 9792–9799, https://doi.org/10.1039/C3CP50393C.
[38] J.J. Lee, C.-H. Chen, D. Shimon, S.E. Hayes, C. Sievers, C.W. Jones, Effect of humidity on the CO_2 adsorption of tertiary amine grafted SBA-15, J. Phys. Chem. C. 121 (42) (2017) 23480–23487, https://doi.org/10.1021/acs.jpcc.7b07930.
[39] M.W. Hahn, M. Steib, A. Jentys, J.A. Lercher, Mechanism and kinetics of CO_2 adsorption on surface bonded amines, J. Phys. Chem. C. 119 (2015) 4126–4135, https://doi.org/10.1021/jp512001t.
[40] M.W. Hahn, J. Jelic, E. Berger, K. Reuter, A. Jentys, J.A. Lercher, Role of amine functionality for CO_2 chemisorption on silica, J. Phys. Chem. B. 120 (8) (2016) 1988–1995.
[41] I. Durán, N. Álvarez-Gutiérrez, F. Rubiera, C. Pevida, Biogas purification by means of adsorption on pine sawdust-based activated carbon: Impact of water vapor, Chem. Eng. J. 353 (2018) 197–207, https://doi.org/10.1016/j.cej.2018.07.100.
[42] Y. Li, H. Yi, X. Tang, F. Li, Q. Yuan, Adsorption separation of CO_2/CH4 gas mixture on the commercial zeolites at atmospheric pressure, Chem. Eng. J. 229 (2013) 50–56, https://doi.org/10.1016/j.cej.2013.05.101.
[43] B. Wadi, A. Mahomed, Y. Bai, A. Osatiashtiani, V. Manovic, S.A. Nabavi, Formulation, adsorption performance, and mechanical integrity of triamine grafted binder-based mesoporous silica pellets for CO2 capture, Powder Technol. 393 (2021) 257–264, https://doi.org/10.1016/j.powtec.2021.07.033.